Heterogeneities in electricity grids strongly enhance non-Gaussian features of frequency fluctuations under stochastic power input

Matthias F. Wolff 🆔, Katrin Schmietendorf, Pedro G. Lind 🆔, Oliver Kamps, Joachim Peinke 🆔, and Philipp Maass 🆔

COLLECTIONS

Paper published as part of the special topic on Dynamics of Modern Power Grids
Note: This paper is part of the Focus Issue on the Dynamics of Modern Power Grids.

View Online   Export Citation   CrossMark

AIP Author Services
English Language Editing

Heterogeneities in electricity grids strongly enhance non-Gaussian features of frequency fluctuations under stochastic power input

Matthias F. Wolff,[1,a] (ID) Katrin Schmietendorf,[2] Pedro G. Lind,[3] (ID) Oliver Kamps,[2,b] Joachim Peinke,[4] (ID) and Philipp Maass[1,c] (ID)

AFFILIATIONS

[1] Fachbereich Physik, Universität Osnabrück, Barbarastraße 7, 49076 Osnabrück, Germany
[2] Institut für Theoretische Physik, Westfälische Wilhelms-Universität Münster, Wilhelm-Klemm-Straße 9, 48149 Münster, Germany
[3] Department of Computer Science, OsloMet—Oslo Metropolitan University, Pilestredet 35, 0166 Oslo, Norway
[4] Institut für Physik & ForWind, Universität Oldenburg, Küpkersweg 70, 26129 Oldenburg, Germany

Note: This paper is part of the Focus Issue on the Dynamics of Modern Power Grids.
[a] **Electronic mail:** mawolff@uos.de
[b] **Current address:** Center for Nonlinear Science, WWU Münster, Corrensstraße 2, 48149 Münster, Germany.
[c] **Electronic mail:** maass@uos.de

ABSTRACT

Stochastic feed-in of fluctuating renewable energies is steadily increasing in modern electricity grids, and this becomes an important risk factor for maintaining power grid stability. Here, we study the impact of wind power feed-in on the short-term frequency fluctuations in power grids based on an Institute of Electrical and Electronics Engineers test grid structure, the swing equation for the dynamics of voltage phase angles, and a series of measured wind speed data. External control measures are accounted for by adjusting the grid state to the average power feed-in on a time scale of 1 min. The wind power is injected at a single node by replacing one of the conventional generator nodes in the test grid by a wind farm. We determine histograms of local frequencies for a large number of 1-min wind speed sequences taken from the measured data and for different injection nodes. These histograms exhibit a common type of shape, which can be described by a Gaussian distribution for small frequencies and a nearly exponentially decaying tail part. Non-Gaussian features become particularly pronounced for wind power injection at locations, which are weakly connected to the main grid structure. This effect is only present when taking into account the heterogeneities in transmission line and node properties of the grid, while it disappears upon homogenizing of these features. The standard deviation of the frequency fluctuations increases linearly with the average injected wind power.

Published under license by AIP Publishing. https://doi.org/10.1063/1.5122986

Electric energy supply is of utmost importance for industrial companies and private households, and it will become even more relevant in connection with actions taken for mitigating climate change effects. The increasing feed-in of wind and solar power into electricity grids poses new challenges for maintaining their stability. The stochastic nature of wind speeds and solar irradiation yields short-term fluctuations of the local frequencies with possible large deviations from the nominal frequency of the desired synchronous operating state. These large deviations can form nuclei for grid instabilities, which can range from single line overloads to malfunction of larger grid parts.

Short-term frequency stability, therefore, must be assessed under erratic power feed-in. Here, we study this problem for wind power injection. We find that wind power feed-in leads to exponentially decaying tails of local frequency distributions. This implies rare large frequency fluctuations to occur much more frequently than expected from assuming simple Gaussian statistics. Decisive factors for the appearance of the non-Gaussian large frequency fluctuations are the heterogeneities in transmission line and node properties. The non-Gaussian features are much less significant and almost negligible in a homogenized grid.

I. INTRODUCTION

The steadily increasing share of fluctuating wind and solar power in electricity grids raises new questions on the assessment and control of grid stability. To tackle this problem, different aspects and challenges need to be considered and mastered. One aspect is the grid topology, which can be generated artificially by some reasonably developed algorithm, which then allows one to perform an ensemble averaging.[1–5] Another option is to use test grids like those provided by the Institute of Electrical and Electronics Engineers (IEEE).[6,7] It is also possible to analyze specific motifs in a grid,[8,9] or one can try to use real grid structures, which unfortunately are, in general, not provided by the network operating companies. However, there are a number of initiatives, such as open_eGo,[10] SciGrid,[11] and others, which try to obtain real grid structures, based mainly on information taken from Open Street Map. Characteristic features of the grid structure are different for different voltage levels, and a further issue is the modeling between these voltage levels.

Another aspect is the modeling depth that means whether one can rely on a simple quasistationary approach based on power-flow equations[6,12,13] or whether one needs to couple these flow equations to the voltage angle dynamics described by the swing equation with possible further extensions for including dynamics of voltage amplitudes.[4,14] In addition, there exist different models to describe generator and load nodes,[15] and it seems to be relevant to take into account the impact of reactances in the coupling of loads and generators to the grid.[7]

The necessary modeling depth for obtaining reliable results will depend also on the relation of several time scales, such as scales for primary and secondary control, intrinsic dynamical scales, and the scales associated with the fluctuations of renewable energy sources.[5,16–19] To account for these fluctuations, we need good descriptions of the stochastic dynamics of wind and solar power, which involves features coming from atmospheric turbulence and cloud effects and questions related to how specific engineering setups affect the transfer of a physical source, e.g., wind speed, to the injected power.

In quasistationary approaches, the focus is generally on how power flows along transmission lines are modified due to a change in renewable power generation and whether weak points can be identified, where lines become overloaded with high probability.[6,12,13,20–23] Fewer studies are concerned yet with the modified power-flow dynamics caused by fluctuations of wind and solar power on short time scales.[5,16,24] These time scales have to be put in relation to those of external control measures. Sudden large deviations of local frequencies from the nominal value can form nuclei for grid instabilities, which can range from single line overloads to malfunction of larger grid parts, up to cascading failures spanning large fractions of the whole grid. A better understanding of the statistics of local frequency fluctuations under the stochastic input of wind and solar power is needed to develop reliable risk estimates of grid failures and strategies to balance risk factors with investments in higher grid stability. Another aspect of the fluctuating power input is a possible reduction of frequency quality, i.e., the percentage of time where the grid operates in a given frequency range. This can be estimated from distributions of local frequencies.

A challenge in treating short-time dynamics in power grids is how to take into account the effect of the external control measures on longer times scales. For example, in a time period of high average wind speed, the conventional generators in the grid will generate less power than in a period of low average wind speed. This means that the state of conventional generator nodes depends on the average wind speed or wind power level. We introduce a concept in this study, where the grid state is adapted to the average wind power level.

Specifically, we focus on the distribution of short-time local frequency fluctuations in the IEEE Reliability Test System 1996 (IEEE RTS-96)[25] if one of its conventional generator nodes is replaced by a node with power feed-in from a wind farm (see Fig. 1). For this feed-in, we take data of wind velocities measured at a tower in the North Sea with a sampling rate of 1 Hz.[26] Both the generator and load nodes of the IEEE-RTS-96 are described by the synchronous machine model. The voltage angle dynamics is determined by the swing equation with forcing by the imbalance of mechanical and electric power. The latter is given by the nonlinear power flow equations, where voltage magnitudes are considered to be fixed.

We also investigate how the distributions of local frequency fluctuations change if transmission line and node heterogeneities in the IEEE-RTS-96 are homogenized by an averaging procedure. Homogenized grid properties are often used in simplified modelings because they reduce the computational effort for solving the nonlinear dynamical equations and make it easier to find fixed point solutions and to maintain numerical stability. However, the use of homogenized grid properties may lead to an underestimation of failure probabilities and a wrong identification of weak parts in the grid.[7]

As a key result of our study, we find that the distributions of local frequency exhibit non-Gaussian features due to tails with approximately exponential decay. These non-Gaussian features can be very pronounced at certain grid nodes. For small frequency fluctuations, the distributions have a nearly Gaussian shape. This Gaussian core part of the distributions gives essentially the fluctuation width, i.e., the standard deviation of frequency fluctuations, while the nearly exponential tails are important for estimating probabilities of rare large fluctuations. In the homogenized grids, the non-Gaussian features are less pronounced and the fluctuation widths are much smaller.

The paper is organized as follows. In Sec. II A, we introduce the basic dynamical equations and the essential features of the IEEE-RTS-96 structure relevant for this study. In Sec. II B, we describe the stochastic wind power generation based on the measured wind speed data, and in Sec. II C, we discuss the wind power feed-in. Our results for the local frequency distributions are detailed in Sec. III. Section IV closes our work with a discussion of the implications of our findings and an outlook for further research.

II. POWER FLOW, STOCHASTIC INPUT, AND GRID STRUCTURE

A. Power-flow dynamics

We model the power-flow dynamics based on the widely[1,3–5,27–29] used synchronous machine model for loads and generators.[15,30,31] With the nominal frequency f_r (50 Hz in Europe) and corresponding angular frequency $\omega_r = 2\pi f_r$, the voltage at node j is $V_j(t) = |V_j| \, \mathrm{Re}\,[e^{-i\omega_r t + i\theta_j(t)}]$, where $\theta_j(t)$ is the phase angle describing the deviation from the synchronous state of operation; the moduli
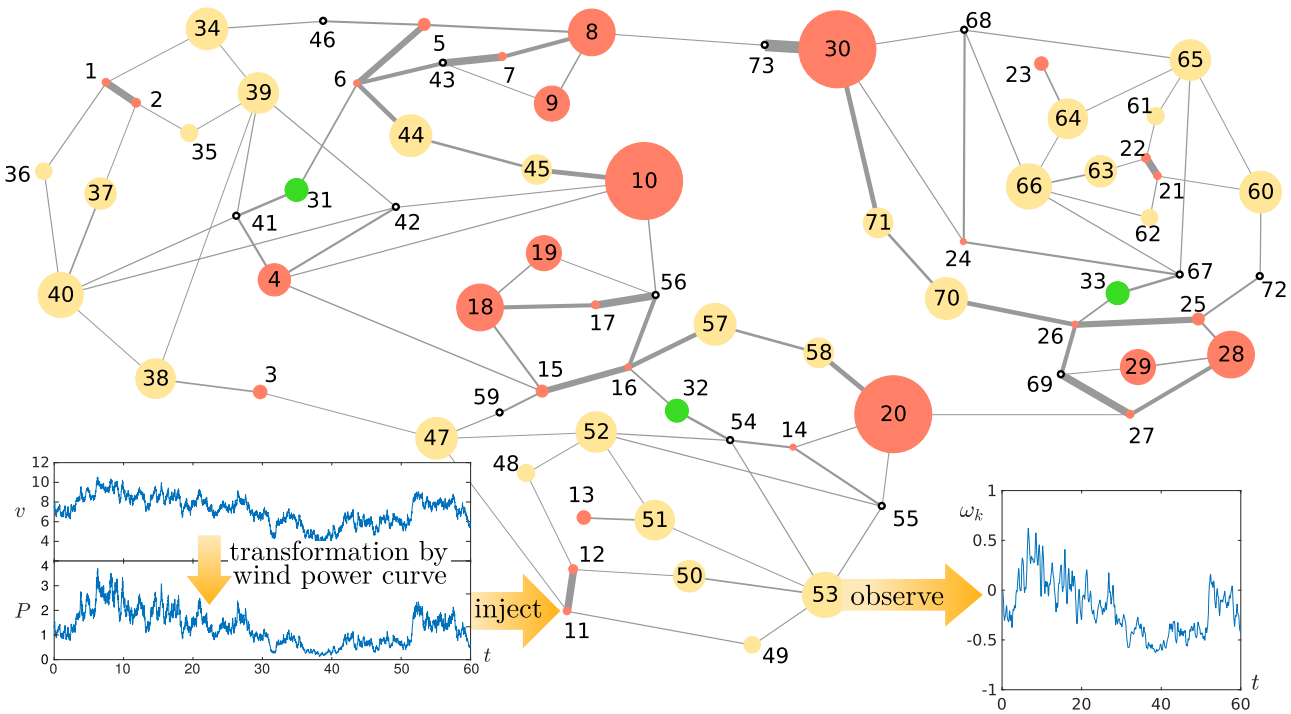
FIG. 1. Sketch of the IEEE RTS-96, consisting of 30 generators labeled from 1 to 30 (red circles), 3 synchronous condensers labeled 31, 32, 33 (green circles), and 40 load nodes labeled from 34 to 73 (yellow circles/open white circles). The small white circles refer to load nodes with vanishing mechanical power. The synchronous condensers have a fixed size, and the size of other symbols has been scaled proportional to their mechanical power. The nodes are connected by 108 transmission lines, where the thickness of the lines marks the strength (modulus) of the respective complex admittances. The insets illustrate the injection of wind power at node 11 due to fluctuating wind speeds $v(t)$ and resulting fluctuations of the frequency ω_k at node $k = 53$.

$|V_j|$ of the voltages are considered to be time-independent. The imbalance $(P_j^{(m)} - P_j)$ between the "mechanical" powers $P_j^{(m)}$ and electrical powers P_j drives the phase angle θ_j according to the swing equation

$$H_j \ddot{\theta}_j + D_j \dot{\theta}_j = P_j^{(m)} - P_j$$
$$= P_j^{(m)} - \sum_k K_{jk} \sin\left(\theta_j - \theta_k - \gamma_{jk}\right). \quad (1)$$

Here, the coupling constants are $K_{jk} = |V_j||V_k||Y_{jk}|$, where $Y_{jk} = |Y_{jk}| \exp[i(\gamma_{jk} + \pi/2)]$ are the elements of the grid admittance matrix Y. H_j are inertia constants of the synchronous machines, i.e., connected with the rotating mass of a conventional generator or motor. The damping constants D_j effectively account for primary control measures,[32] which drives the grid into a synchronous state of operation. From a mechanical perspective, Eq. (1) correspond to a Newtonian dynamics of nonlinearly coupled oscillators with damping. These are often referred to as the "second-order Kuramoto equations".[33–35]

We have solved the swing equations (1) numerically by applying a Runge-Kutta solver of fourth order with a time step of 5×10^{-4} s. As for the parameters, listed values for the IEEE RTS-96 were used and estimates for the H_j, D_j based on the findings reported in Ref. 36. For a comparison with a simplified homogenized grid variant,

arithmetic means of line admittances as well as of consumed and generated powers are taken. A detailed description of all parameters is given in Ref. 7.

If the mechanical powers $P_j^{(m)}$ do not fluctuate, a stationary synchronous state of the grid develops after some transient time, where all frequency deviations $\omega_j = \dot{\theta}_j$ from the nominal frequency ω_r are zero and all θ_j are constant. In principle, knowing $P_j^{(m)}$ and $K_{jk} = |V_j||V_k||Y_{jk}|$, the phase angles in this state can be calculated by setting the left-hand side of Eq. (1) to zero. However, for load nodes the voltages $|V_j|$ are generally not known but the reactive powers $Q_j^{(m)}$. For determining the synchronous state, we thus have to solve the full power-flow equations

$$P_j^{(m)} = P_j = \sum_k |V_j||V_k||Y_{jk}| \sin\left(\theta_j - \theta_k - \gamma_{jk}\right), \quad (2a)$$

$$Q_j^{(m)} = Q_j = \sum_k |V_j||V_k||Y_{jk}| \cos\left(\theta_j - \theta_k - \gamma_{jk}\right), \quad (2b)$$

which express the balance between mechanical and electrical powers, including Ohmic losses. We solve these equations by the Newton-Raphson method with starting angles $(\theta_1, \ldots, \theta_N) = (0, \ldots, 0)$, yielding a unique fixed point vector $(0, \theta_2^*, \ldots, \theta_N^*)$. Alternatively, one could use the holomorphic embedding load-flow method for

determining the fixed point of synchronous operation.[37] If the mechanical powers are chosen to have values different from the ones listed for the IEEE-RTS-96, we have taken node 4 as the reference bus for determining the fixed point state.

B. Stochastic power generation

In earlier times, where power was produced solely by conventional generators, fluctuations of $P_j^{(m)}$ had to be considered for the load nodes. Typically, the impact of corresponding load fluctuations can be treated in a quasistationary approach based on the power-flow equations (2). This is because significant changes of consumed power occur on time scales large compared to relaxation times to the fixed point state which lie in the range of 3–20 s.[7]

In the presence of stochastic feed-in from renewable energy sources, the impact of fluctuating $P_j^{(m)}$ must be considered also for generator nodes. The dynamics described by Eq. (1) can then no longer be ignored because power feed-in from wind and solar irradiation shows significant changes on short time scales. To account for these fluctuations, corresponding stochastic processes for $P_j^{(m)}(t)$ need to be specified. When inserting these into Eq. (1), the phase angles $\theta_j(t)$ and frequencies $\omega_j(t) = \dot{\theta}_j(t)$ become stochastic processes as well.

In this paper, we focus on the frequency fluctuations under stochastic feed-in of wind power. An important statistical feature of wind speeds is that distributions of velocity increments on even short times of order 1 s exhibit tails much heavier than that of a Gaussian distribution due to the intermittent nature of turbulent flows. Wind speed increments of, for example, 5 m/s are rare but have probabilities that are by several orders higher than those expected from a Gaussian distribution with mean and variance given by the measured data. Recent results suggest that wind speed fluctuations are rather directly reflected in the generated power on short time scales of seconds and below.[17] This would imply that rare events of large sudden power changes could be an important risk factor for maintaining grid stability.

To capture realistic features of the wind, we base our study on a series of wind speeds v measured at a tower located in the North Sea with a sampling rate of 1 Hz.[26] From this series, we take the data $\{v_n\}_{1 \leq n \leq N}$ sampled in October 2016 ($N = 2\,678\,400$) for our study. These wind speeds show strong fluctuations on all time scales. The time window, where the grid state dynamics are described by Eq. (1), is, however, restricted by control measures. The synchronous state of operation generated by primary control can have a frequency that deviates from the nominal value. Secondary control measures tend to restore a synchronous state at the nominal frequency. It involves time-delay feedback and integration of power imbalances on time scales of about 30 s. We here take this secondary control into account in an effective manner by assuming that the ideal synchronous state at the nominal frequency is restored after 1 min. Accordingly, we divide the series $\{v_n\}_{1 \leq n \leq N}$ into subsequent segments of 1 min, yielding in total $N/60 = 44\,640$ sets, as illustrated by the vertical dashed lines in Fig. 2. These sets of 1-min data form the basis for the stochastic wind power input $P_j^{(m)}(t)$ in Eq. (1).

To convert the wind speeds into powers we make use of the so-called "power curve" $P(v)$, which describes how wind speed translates to wind power on average. The power curve $P(v)$ increases
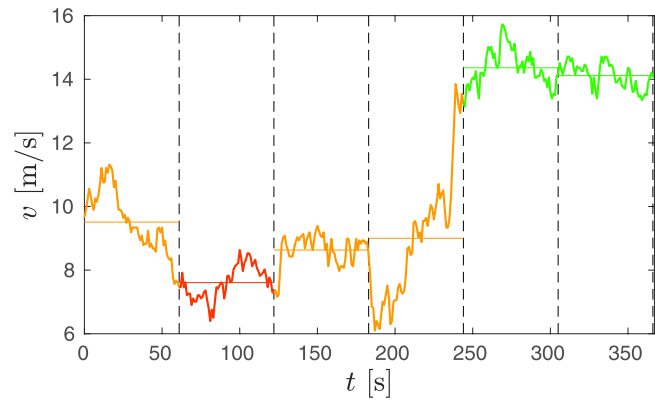
FIG. 2. Section of the wind speed series measured at a tower located in the North Sea with a sampling rate of 1 Hz.[26] The vertical dashed lines indicate the division into segments of 1 min. Data are colored differently with respect to the mean wind speed in each segment (horizontal lines), corresponding to a grouping into bins of widths 2 m/s, see the discussion in Sec. III.

nearly as $\propto v^3$ for small v up to a rated velocity v_r, where the power reaches its maximal allowed value P_r to prevent the wind turbines from getting damaged (pitch control), see Fig. 3. The data points in this figure are taken from Ref. 38, and the solid line is a cubic fit to the data for small v with a crossover to constant P_r for $v \geq v_r$. The rated speed $v_r = 12.5$ m/s was determined from the average $\langle v \rangle$ of the measured speeds $\{v_n\}_{1 \leq n \leq N}$ and by applying the rule of thumb $v_r = 1.5 \langle v \rangle$.[39] Let us note that the power curve has a "cut-in speed" at about 4 m/s, and a "cut-off speed" at about 25 m/s, above which
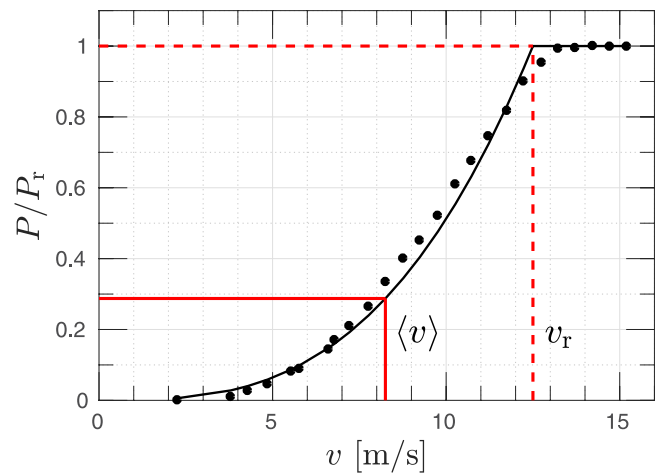
FIG. 3. Power curve giving the dependence of the average wind power P on the wind speed v. The power is normalized to the rated value P_r, which is the saturation value for speeds larger than the rated speed v_r. The data points are extracted from Ref. 38, and the solid black line is a cubic fit to the data for $v < v_r$. The solid red line indicates the mean value $\langle v \rangle$ of the wind speeds sampled in October 2016 at the tower in the North Sea[26] and its corresponding power.

the blades of a wind turbine are turned away from the wind and the power drops to zero. In our subsequent analysis, we consider only sets of 1-min data with mean wind speeds between 4 m/s and 18 m/s.

When substituting a conventional generator j in the IEEE-RTS-96 by a wind farm, we also need to specify the size of the farm. This is done by demanding the power generated at the mean wind speed $\langle v \rangle$ to be equal to the power P_j^{conv} of the substituted conventional generator. Accordingly, the translation of wind speed v into wind power $P_j^{\mathrm{w}}(v)$ at node j is

$$P_j^{\mathrm{w}}(v) = \begin{cases} \dfrac{P_j^{\mathrm{conv}}}{\langle v \rangle^3} v^3, & v \leq v_{\mathrm{r}}, \\ (P_{\mathrm{r}})_j, & v \geq v_{\mathrm{r}}, \end{cases} \tag{3}$$

with $(P_{\mathrm{r}})_j = P_j^{\mathrm{conv}} v_{\mathrm{r}}^3 / \langle v \rangle^3$.

The measured wind speed data $\{v_n\}_{1 \leq n \leq N}$ have a time resolution of 1 s. Much shorter time resolutions of order 1 ms are necessary to integrate Eq. (1) with numerical accuracy. In order to specify a time-continuous stochastic process for the feed-in of wind power in Eq. (1), one could use a step-function approach, e.g., by defining $v(t) = v_1 + \sum_{n=1}^{N-1} (v_{n+1} - v_n) \Theta(t - n)$ with $\Theta(.)$, the Heaviside jump function [$\Theta(x) = 1$ for $x \geq 0$ and zero otherwise; t in units of seconds]. However, this approach would ignore fluctuations on shorter scales. We, therefore, prefer to use a stochastic interpolation scheme between consecutive values v_n, v_{n+1} that is explained in the Appendix.

C. Wind power feed-in

As mentioned in the Introduction, it is important to take into account that the external control measures are acting on longer time scales and lead to a state of the controllable generators that is adapted to the average wind power. Therefore, for a given set of 1-min data, we calculate the mean wind power $\bar{P}_j^{\mathrm{w}}$. This average $\bar{P}_j^{\mathrm{w}}$ is, in general, not equal to the nominal power P_j^{conv} of the original conventional generators in the IEEE RTS-96, implying a power imbalance between the total generated power and the sum of the total consumed power $|P_{\mathrm{tot}}^{\mathrm{load}}| = -P_{\mathrm{tot}}^{\mathrm{load}}$ (assumed to be fixed) and the Ohmic losses.

However, due to the external control measures, we can view the conventional generators to be uniformly scaled, $P_k^{\mathrm{conv}} \rightarrow \beta P_k^{\mathrm{conv}}$ so that the total power generation ($\bar{P}_j^{\mathrm{w}} + \beta \sum_{k \neq j} P_k^{\mathrm{conv}}$) averaged over 1 min remains the same as in the unmodified IEEE-RTS-96. The scale factor β is

$$\beta = \frac{\sum_l P_l^{\mathrm{conv}} - \bar{P}_j^{\mathrm{w}}}{\sum_{k \neq j} P_k^{\mathrm{conv}}}. \tag{4}$$

Given $\bar{P}_j^{\mathrm{w}}$ and $\beta P_k^{\mathrm{conv}}$ for $k \neq j$, the correspondingly modified IEEE-RTS-96 assumes a new fixed point, which we determine as described in Sec. II A. To solve Eq. (1) for a given 1-min realization of the feed-in process, we always start in this fixed point state, thereby effectively taking into account the adaptation of the state due to external control measures.

III. LOCAL FREQUENCY DISTRIBUTIONS

The numerical solutions of the swing equations allow us to determine the local rates $\omega_k = \dot{\theta}_k$ of phase angle changes. We refer to these deviations simply as "local frequencies" in the following. Their distributions are analyzed in this section.

To identify possible differences for periods of weak and strong wind, we perform our analysis conditioned on the average wind speed in 1-min intervals. Thus, we introduce bins, where the wind speed averaged over 1 min lies in ranges 4–6 m/s, 6–8 m/s, ..., 18–20 m/s. A section of the wind speed series $v(t)$ is shown in Fig. 2, where we have also indicated the division into 1-min segments (each having its own 1-min average wind speed). The wind speed series $v(t)$ is transformed into a power series $P_j^{\mathrm{w}}(t)$ as described above.

Within the 1-min intervals, the wind speed shows strong fluctuations, including sudden changes reflecting its intermittent nature. This is demonstrated in Fig. 4(a), where we show the distributions $\psi(\Delta v)$ of 1-s wind speed increments $\Delta v = v(t + 1) - v(t)$ obtained from a sampling restricted to all 1-min sections with average wind speeds in the bin 8-10 m/s. These distributions show the typical heavy tails reflecting the intermittent behavior: large wind speed changes
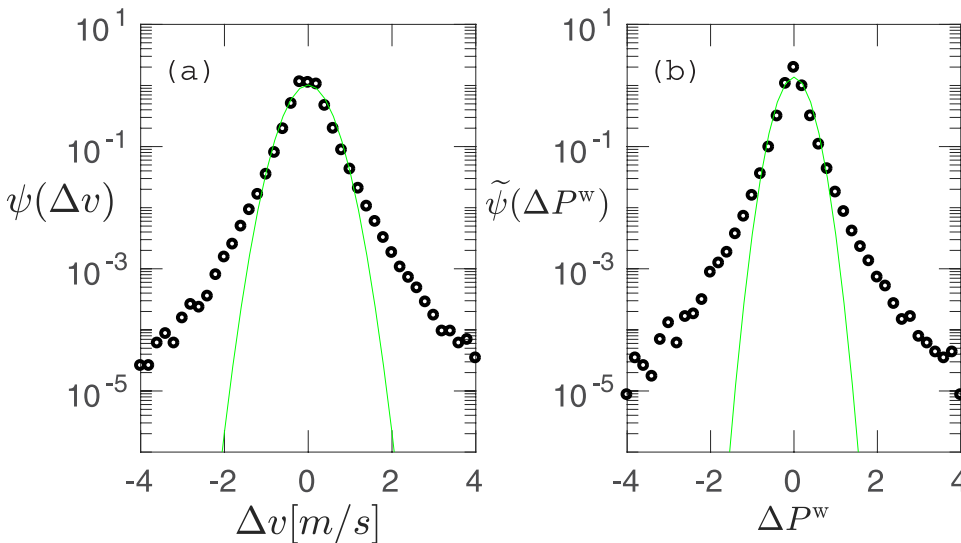

FIG. 4. (a) Distribution $\psi(\Delta v)$ of 1-s increments Δv of wind speeds obtained from the time series measured at a tower in the North Sea. In the sampling, only those data are included, where the average wind speed in a 1-min time interval lies in the range 8–10 m/s. (b) Corresponding distribution $\widetilde{\psi}(\Delta P^{\mathrm{w}})$ of increments of wind power feed-in at node $j = 13$ that result from the transformation of wind speeds into powers described in Sec. II B. The green lines in both graphs correspond to Gaussian distributions with zero mean and the same standard deviation as that of $\psi(\Delta v)$ and $\widetilde{\psi}(\Delta P^{\mathrm{w}})$.

occur much more frequently than expected from a Gaussian distribution [green line in Fig. 4(a)]. The heavy tails in the distribution of wind speed increments are rather directly transformed into heavy tails of the distribution of wind power increments [see Fig. 4(b)].

Figure 5(a) displays an example of a histogram of frequencies, which was obtained for one realization of 1-min wind power feed-in at node 13 with a mean wind speed belonging to the bin 8–10 m/s [corresponding to the distribution of wind power increments shown in Fig. 4(b)]. For this histogram, the local frequencies at all other nodes were sampled. The shape of the histogram can be described by a Gaussian core part for small frequencies (solid green line) and a nearly exponential tail behavior for large frequencies (for both positive and negative deviations from the nominal frequency). It is interesting to compare this histogram with the one for the homogenized grid structure when exactly the same sequence of 1-min wind power data is injected at node 13. The corresponding histogram is shown in Fig. 5(b). Its shape can be described in the same way, but the Gaussian core part has a much smaller width and the exponential tails decay more rapidly.

When investigating other 1-min sets of wind power data and/or other injection nodes, we obtain histograms of similar shape, which can be characterized by a Gaussian core and exponential tail part. This holds true irrespective of the scale of average wind speed, i.e. irrespective of the bin, to which the set of 1-min wind power data is assigned. That similar histogram shapes are obtained for all 1-min sets is somewhat surprising in view of the intermittent wind speed behavior, which is reflected in occasional jumplike changes of the wind speed in short time intervals. For example, consider the 1-min set of wind speed data between 120 s and 180 s and the following set between 180 s and 240 s in Fig. 2. In the former set, the wind speeds show only small fluctuations around the mean wind speed. In the latter set, by contrast, jumplike changes are seen at its beginning and

end, and between these sudden changes there is a strong overall drift from smaller wind speeds of order 6 m/s to larger values of about 10 m/s. The differences in the behaviors of the wind speed thus do not translate into distinct types of histogram shapes but a different significance of the Gaussian core and exponential tail part.

We quantify the differences by introducing two parameters. The first is the standard deviation σ of the local frequency fluctuations, whose value is largely determined by the Gaussian core part. In fact, the solid green lines in Figs. 5(a) and 5(b) correspond to a Gaussian distribution with zero mean and standard deviation σ. The second parameter is

$$\alpha = \frac{\langle \omega^4 \rangle}{3\sigma^4} - 1, \tag{5}$$

which is commonly referred to as the non-Gaussian parameter in the literature. For a Gaussian distribution one finds $\alpha = 0$, while the exponential tails lead to $\alpha > 0$, i.e., this parameter quantifies the significance of the non-Gaussian tails.

For the histogram in Fig. 5(a), we find $\sigma = 0.13$ and $\alpha = 2.83$, while for the corresponding histogram of the homogenized grid in Fig. 5(b), $\sigma = 0.06$ and $\alpha = 0.36$. The intermittent nature of the wind must be reflected in variations of σ and α for different 1-min data sets. These variations are exemplified in the graphs right to the histograms shown in Figs. 5(a) and 5(b) for 100 sets belonging to the same bin 8–10 m/s of average wind speed. The mean values $\bar{\sigma}_j$ and $\bar{\alpha}_j$ are indicated by the horizontal green lines in these graphs.

So far, we have considered just one injection node $j = 13$. To investigate how the $\bar{\sigma}$ and $\bar{\alpha}$ vary with the location of wind power feed-in, we have determined, for the same hundred sets taken for Figs. 5(a) and 5(b), the $\bar{\sigma}_j$ and $\bar{\alpha}_j$ for all replacements of conventional generator nodes $j = 1, \ldots, 30$ by a wind farm. The results, are shown in Figs. 6 and 7.
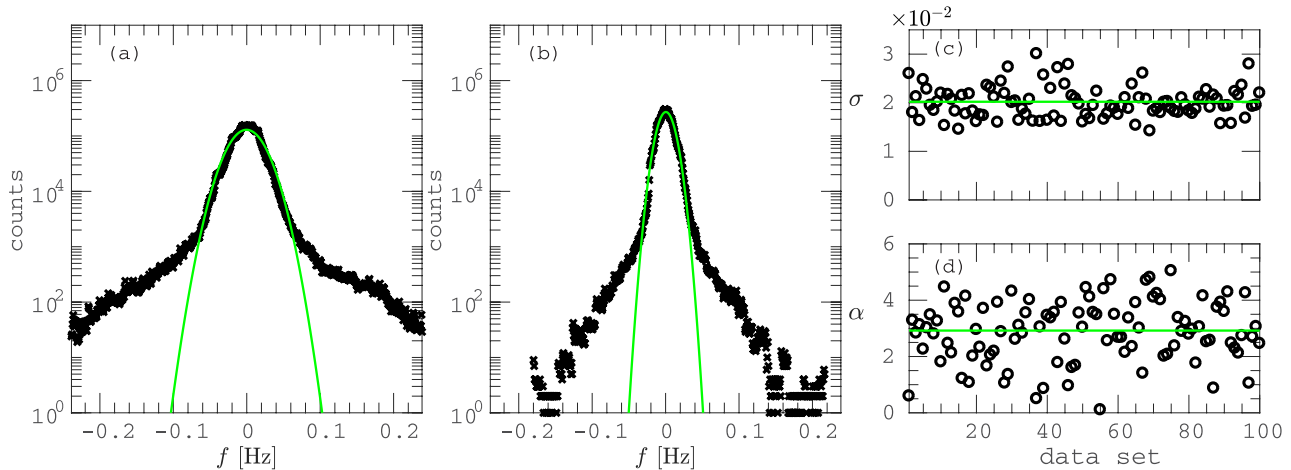
FIG. 5. Example of local frequency histograms (black crosses) for a 1-min wind power feed-in $P^w(t)$ at node 13 whose mean wind speed $\bar{P}^w$ belongs to the bin 8–10 m/s, (a) for the IEEE RTS-96 (after replacement of node 13 for wind-power feed-in) and (b) for the corresponding homogenized grid structure (as described in Sec. II A). Frequency data were sampled at all other nodes. The green lines correspond to Gaussian distributions with zero mean and standard deviation σ calculated from the frequency fluctuations. The graphs (c) and (d) depict variations of σ and the non-Gaussian parameter α [defined in Eq. (5)] for different 1-min power feed-in at the same node $j = 13$. The horizontal green lines show the average values. Non-Gaussian parameters for the homogeneous grid variant are much smaller (cf. Fig. 6).
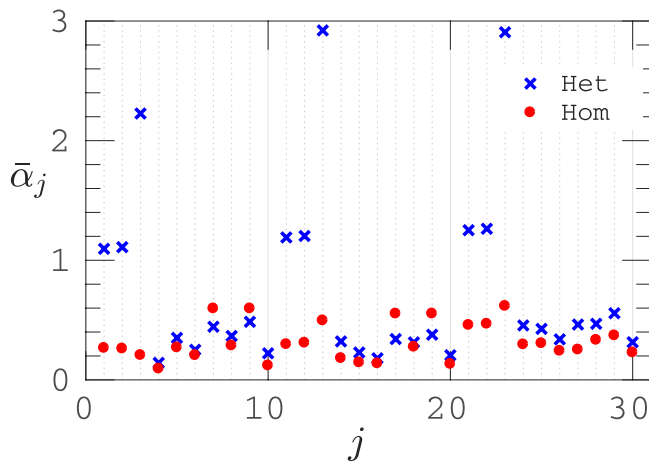
FIG. 6. Mean non-Gaussian parameter $\bar{\alpha}_j$ for the different wind injection nodes $j = 1, \ldots, 30$ in the bin of mean wind velocities 8–10 m/s. For each injection node, the averaging was performed over the same hundred 1-min sets of wind speed data. Blue crosses mark the results for the heterogeneous grid structure, and red circles for the homogenized variant.

In Fig. 6, we see that there are two injection nodes $j = 13$ and 23 in the heterogeneous grid (blue crosses) with a large $\alpha_j \simeq 3$. When looking for peculiarities of these nodes, we find that they are the only dead-ends in the IEEE-RTS-96, see Fig. 1. In the homogenized grid, this effect of dead-ends is not significant and all $\alpha_j \lesssim 0.6$ (red circles in Fig. 6).

For most of the other injection nodes j in the heterogeneous grid, we also find $\alpha_j \lesssim 0.6$, with some further exceptions: Node $j = 3$ with $\alpha_j \simeq 2.2$ is effectively a dead-end with one strong link to node 38 and a comparatively much weaker link to node 47. Nodes 1, 2, 11, 12, 21, and 22 with $\alpha_j \gtrsim 1$ all belong to strongly linked pairs (1,2), (11,12), and (21,22) that are only weakly linked to other nodes. For other bins than the 8–10 m/s bin discussed here, the same nodes

j are identified as those with particular large $\bar{\alpha}_j$ values. Large non-Gaussian parameters thus occur for injection nodes that are weakly connected to the entire grid structure.

Interestingly, dead-ends were reported as a potentially destabilizing factor of power grids also when analyzing the attraction basin of fixed points of Eq. (1) under frequency and voltage angle perturbations.[1,7] Moreover, the pattern of $\bar{\alpha}_j$ seen in Fig. 6 for the heterogeneous case correlates strongly with an estimation of probabilities of wind injection nodes to give rise to transmission line overloads.[6] This a remarkable finding, as the estimation of these overload probabilities was based on a quasistationary approach, i.e., without considering the complex nonlinear dynamics given by Eq. (1).

The data for the standard deviation $\bar{\sigma}_j$ in Fig. 7(a) show again that the homogenized variant misses to capture important features of the dynamics seen in the heterogeneous grid structure. While $\bar{\sigma}_j \simeq 0.07$ for all nodes in the homogenized variant, $\bar{\sigma}_j$ in the heterogeneous grid are always larger and vary significantly between different injection nodes, attaining up to four times larger values. These variations of $\bar{\sigma}_j$ are not related to peculiar topological features but are simply connected to the mean wind power injected at node j i.e., to the size of the wind farm, see the discussion in Sec. II B. The relation is demonstrated in Fig. 7(b), where we plotted $\bar{\sigma}_j$ against $P_j^{\mathrm{w}}(v_c)$ from Eq. (3), with $v_c = 9$ m/s the wind speed in the center of the considered bin. The linear relation between $\bar{\sigma}_j$ and $P_j^{\mathrm{w}}(v_c)$ is valid also for the other bins of average wind speed.

IV. SUMMARY, CONCLUSIONS AND OUTLOOK

In summary, we have developed an approach to access the impact of short-term fluctuations of wind speed and associated wind power on local frequency fluctuations in power grids. For our analysis, we used the swing equations by applying a synchronous machine model for all nodes. We accounted for external control measures by adjusting the grid state to the average power feed-in on a time scale of 1 min. Wind speeds were translated into wind power by resorting
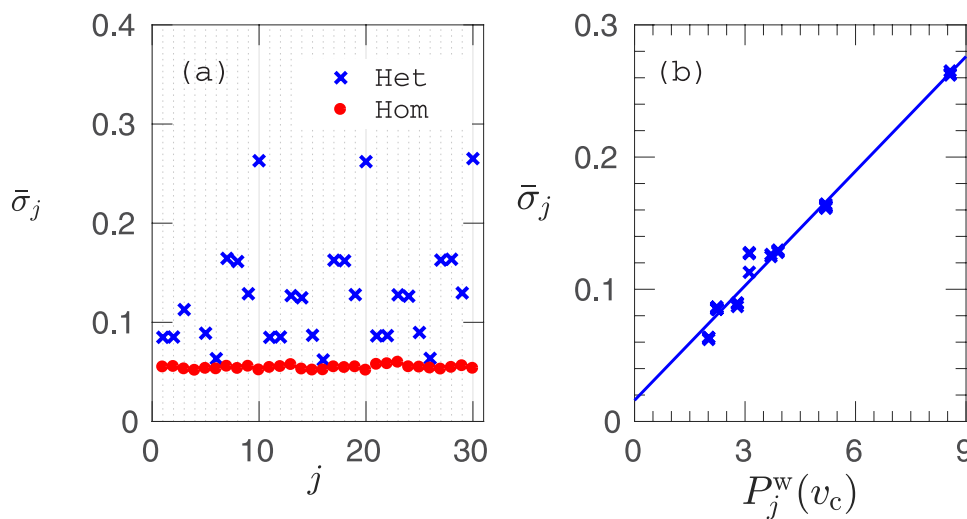
FIG. 7. (a) Mean values $\bar{\sigma}_j$ of the standard deviation for the different wind injection nodes $j = 1, \ldots, 30$ in the bin of mean wind velocities 8–10 m/s. Blue crosses mark the results for the heterogeneous grid structure, and red circles for the homogenized variant. (b) Linear relation between $\bar{\sigma}_j$ and $P_j^{\mathrm{w}}(v_c)$ [cf. Eq. (3)] with $v_c = 9$ m/s being the wind speed in the bin center.

to the so-called power curve. We considered single-node injection of wind power at different locations in the IEEE-RTS-96 by replacing one of its conventional generator nodes with a wind farm. The wind farm size was adjusted to the power of the replaced conventional generator. Modeling of the wind speeds was based on measured data at a tower in the North Sea with a time resolution of 1 s and a stochastic interpolation to smaller time steps used for integrating the swing equations. In addition, we studied the consequences of homogenizing transmission line and node properties.

We found that histograms of local frequency deviations from the nominal frequency of the synchronous state exhibit a common type of shape, which we could describe by a Gaussian distribution for small frequency deviations and an approximately exponentially decaying tail part. Without attempting to fit the shape of each individual of the about 10^4 histograms investigated, we quantified the relevant features by introducing just two parameters: (i) the standard deviation of the local frequency fluctuation, which is largely determined by the Gaussian core part and (ii) the non-Gaussian parameter [Eq. (5)], which is sensitive to the tail part. The non-Gaussian parameter can assume large values in the heterogeneous grid for injection nodes weakly connected to the entire grid, in particular, those forming dead-ends. This indicates that these injection nodes are more likely to cause large local frequency fluctuations. These large fluctuations should be avoided as they can nucleate severe grid failures. In a homogenized grid variant, the "dead-end effect" is not significant. The standard deviations showed strong variations from node to node. They turned out to be essentially proportional to the magnitude of the average wind power injection. In agreement with this observation, the standard deviations were almost the same for all wind power injection nodes in the homogenized grid variant.

We consider our study to be just a first step for a better understanding of the impact of short-term fluctuations of wind energy on the stability of power grids. An important task is to investigate to which extent different possible origins contribute to the non-Gaussian features and whether one can identify a dominating one. To this end, it will be useful to separate effects associated with (i) the nonlinearities in the swing equations [Eq. (1)] , (ii) the saturation of the power curve [Eq. (3)], and (iii) the non-Gaussian wind statistics, in particular, its intermittent nature implied by atmospheric turbulence, as reflected in the increment distributions shown in Figs. 4(a) and 4(b). In this context, improvements in the modeling should be implemented for a more realistic stochastic translation of wind speed into power[38] and a better modeling of the wind injection, e.g., by using measured data with finer resolution (if available), or by applying reliable models for generating surrogate data, or by improving the stochastic interpolation method between measured data. Further developments should also include a more realistic representation of the load nodes, e.g., by using the effective network or structure preserving model,[15] as well as an account for the modified dynamics implied by the ac/dc and dc/ac inverters used for the wind power feed-in. The swing Eq. (1) can be modified to take into account secondary control measures also,[40] which would allow one to extend the analysis to longer time scales.

Going along with these improvements in the grid modeling, extended setups of the wind power feed-in need to be studied and the analysis of stochastic grid dynamics should be widened. As

for the wind power feed-in, higher penetrations of the grid with wind power must be investigated under consideration of both spatial and temporal correlations of wind velocities. As for the analysis of stochastic grid dynamics, it is important to quantify correlations between local frequency fluctuations. Preliminary results for distributions of frequency increments show similar features as reported for the histograms of the frequencies themselves.

APPENDIX: STOCHASTIC INTERPOLATION

Let v_0 and v_1 be two of the measured wind speeds separated by 1 s. Defining two stochastic processes $v_+(t)$ and $v_-(t)$, $t \in [0, 1]$, with starting values $v_+(0) = v_0$, $v_-(0) = v_1$, a stochastic interpolation between v_0 and v_1 is given by

$$v(t) = (1 - t)v_+(t) + tv_-(1 - t), \quad t \in [0, 1]. \quad (A1)$$

Hence, the process $v_+(t)$ is considered to run forward in time and to contribute to $v(t)$ with weight $(1 - t)$, while the process $v_-(t)$ runs backward in time and contributes with weight t.

Specifically, we use here a simple Ornstein-Uhlenbeck process for $v_\pm(t)$, i.e., $v_\pm(t)$ obey the Langevin equations

$$\frac{dv_\pm(t)}{dt} = -\gamma[v_\pm(t) - \bar{v}_\pm(t)] + \sqrt{2\Gamma}\,\eta(t), \quad (A2)$$

where $\eta(t)$ is a Gaussian white noise with zero mean and correlator $\langle\eta(t)\eta(t')\rangle = \delta(t - t')$. Based on studies of correlation properties of the measured time series $\{v_n\}_{1 \leq n \leq N}$,[41] we set γ to 0.54 and $\Gamma = \gamma/2$. The time-dependent mean values $\bar{v}_\pm(t)$ are $\bar{v}_+(t) = \bar{v}_-(1 - t) = \bar{v}(t)$, where

$$\bar{v}(t) = v_0 + (v_1 - v_0)t, \quad t \in [0, 1], \quad (A3)$$

is the linear interpolation between v_0 and v_1. Hence, the Ornstein-Uhlenbeck processes $v_+(t)$ and $v_+(1 - t)$ in Eq. (A1) are biased toward the linearly interpolated value at all intermediate times t.

The Langevin equations (A2) are integrated to yield a stochastic sequence $v(n\Delta t)$, $n = 1, \ldots, (1/\Delta t - 1)$, of wind speeds between v_0 and v_1 with time resolution Δt, where in our case $\Delta t = 5 \times 10^{-4}$ s.

REFERENCES

[1]P. Menck, J. Heitzig, J. Kurths, and H. Schellnhuber, Nat. Commun. **5**, 3969 (2014).
[2]P. Schultz, J. Heitzig, and J. Kurths, Eur. Phys. J. Spec. Top. **223**, 2593 (2014).
[3]D. Jung and S. Kettemann, Phys. Rev. E **94**, 012307 (2016).
[4]S. Auer, K. Kleis, P. Schultz, J. Kurths, and F. Hellmann, Eur. Phys. J. Spec. Top. **225**, 609 (2016).
[5]S. Auer, F. Hellmann, M. Krause, and J. Kurths, Chaos **27**, 127003 (2017).
[6]C. Schiel, P. G. Lind, and P. Maass, Sci. Rep. **7**, 11562 (2017).
[7]M. F. Wolff, P. G. Lind, and P. Maass, Chaos **28**, 103120 (2018).
[8]P. Schultz, J. Heitzig, and J. Kurths, New J. Phys. **16**, 125001 (2014).
[9]H. Kim, S. H. Lee, J. Davidsen, and S.-W. Son, New J. Phys. **20**, 113006 (2018).

[10] U. P. Müller, L. Wienholt, D. Kleinhans, I. Cussmann, W.-D. Bunke, G. Pleßmann, and J. Wendiggensen, J. Phys. Conf. Ser. **977**, 012003 (2018).

[11] W. Medjroubi and C. Matke, *SciGRID—An Open Source Reference Model for the European Transmission Network (v0.2)* (2016).

[12] M. Anghel, K. A. Werley, and A. E. Motter, *40th Annual Hawaii International Conference on System Sciences (HICSS'07)* (IEEE Computer Society, 2007), pp. 113–113.

[13] M. Chertkov, M. Stepanov, F. Pan, and R. Baldick, in *Proceedings of the 50th IEEE Conference on Decision and Control and European Control Conference, CDC-ECC 2011, Orlando, FL, USA* (IEEE, 2011), pp. 2174–2180.

[14] K. Schmietendorf, J. Peinke, R. Friedrich, and O. Kamps, Eur. Phys. J. Spec. Top. **223**, 2577 (2014).

[15] T. Nishikawa and A. Motter, New J. Phys. **17**, 015012 (2015).

[16] K. Schmietendorf, J. Peinke, and O. Kamps, Eur. Phys. J. B **90**, 222 (2017).

[17] H. Hähne, J. Schottler, M. Wächter, J. Peinke, and O. Kamps, Europhys. Lett. **121**, 30001 (2018).

[18] H. Hähne, K. Schmietendorf, S. Tamrakar, J. Peinke, and S. Kettemann, Phys. Rev. E **99**, 050301 (2019).

[19] B. Schäfer, C. Beck, K. Aihara, D. Witthaut, and M. Timme, Nat. Energy **3**, 119 (2018).

[20] R. Albert, I. Albert, and G. L. Nakarado, Phys. Rev. E **69**, 025103 (2004).

[21] J.-W. Wang and L.-L. Rong, Saf. Sci. **47**, 1332 (2009).

[22] P. Hines, E. Cotilla-Sanchez, and S. Blumsack, Chaos **20**, 033122 (2010).

[23] M. Andrychowicz and B. Olek, in *13th International Conference on the European Energy Market (EEM)* (IEEE, 2016), pp. 1–5.

[24] K. Schmietendorf, O. Kamps, M. Wolff, P. G. Lind, P. Maass, and J. Peinke, "Bridging between load-flow and Kuramoto-like power grid models: A flexible approach to integrating electrical storage units," e-print arXiv:1812.01972, 2018.

[25] C. Grigg, P. Wong, P. Albrecht, R. Allan, M. Bhavaraju, R. Billinton, Q. Chen, C. Fong, S. Haddad, S. Kuruganty *et al.*, IEEE Trans. Power Syst. **14**, 1010 (1999).

[26] FINO I Project and Database (2016). The FINO project is supported by the German Government through BMWi and PTJ. See http://www.bsh.de.

[27] M. Rohden, A. Sorge, M. Timme, and D. Witthaut, Phys. Rev. Lett. **109**, 064101 (2012).

[28] B. Schäfer, D. Witthaut, M. Timme, and V. Latora, Nat. Commun. **9**, 1975 (2018).

[29] S. Tamrakar, M. Conrath, and S. Kettemann, Sci. Rep. **8**, 6459 (2018).

[30] J. Machowski, J. Bialek, and J. Bumby, *Power System Dynamics* (John Wiley & Sons, New Jersey, 2008).

[31] G. Filatrella, A. H. Nielsen, and N. F. Pedersen, Eur. Phys. J. B **61**, 485 (2008).

[32] See https://www.entsoe.eu for "UCTE Operation Handbook" (2004).

[33] Y. Kuramoto, *Mathematical Problems in Theoretical Physics*, Lecture Notes in Physics, edited by H. Araki (Springer, Berlin, 1975), Vol. 39, pp. 420–422.

[34] J. A. Acebrón, L. L. Bonilla, C. J. Pérez Vicente, F. Ritort, and R. Spigler, Rev. Mod. Phys. **77**, 137 (2005).

[35] F. A. Rodrigues, T. K. D. Peron, P. Ji, and J. Kurths, Phys. Rep. **610**, 1 (2016).

[36] A. E. Motter, S. A. Myers, M. Anghel, and T. Nishikawa, Nat. Phys. **9**, 191 (2013).

[37] A. Trias, in *IEEE Power and Energy Society General Meeting* (IEEE, 2012), pp. 1–8.

[38] P. Milan, M. Wächter, and J. Peinke, J. Renew. Sustain. Energy **6**, 033119 (2014).

[39] J. F. Manwell, J. G. McGowan, and A. L. Rogers, *Wind Energy Explained* (John Wiley & Sons, 2009).

[40] P. C. Böttcher, A. Otto, S. Kettemann, and C. Agert, "Time delay effects in the control of synchronous electricity grids," e-print arXiv:1907.13370v1, 2019.

[41] M. Brune, "Modeling of wind speeds with the Langevin equation," Bachelor thesis (Osnabrück University, 2018).